Available online at www.sciencedirect.com
SCIENCE DIRECT
Biochimica et Biophysica Acta 1757 (2006) 143 – 153
BIOCHIMICA ET BIOPHYSICA ACTA
BBA
http://www.elsevier.com/locate/bba

Solution structures of tetrahaem ferricytochrome c_3 from *Desulfovibrio vulgaris* (Hildenborough) and its K45Q mutant: The molecular basis of cooperativity

Ana C. Messias [a,1], António P. Aguiar [a,b], Lorraine Brennan [a], Carlos A. Salgueiro [a,c], Lígia M. Saraiva [a], António V. Xavier [a], David L. Turner [a,d,*]

[a] *Instituto de Tecnologia Química e Biológica, Universidade Nova de Lisboa, Rua da Quinta Grande 6, 2780-156 Oeiras, Portugal*
[b] *Instituto Superior Técnico, Universidade Técnica de Lisboa, Avenida Rovisco Pais, 1049-001 Lisboa, Portugal*
[c] *Departamento de Química, Faculdade de Ciências e Tecnologia, Universidade Nova de Lisboa, Quinta da Torre, 2825-114 Caparica, Portugal*
[d] *School of Chemistry, University of Southampton, Southampton SO17 1BJ, UK*

Received 5 December 2005; received in revised form 17 January 2006; accepted 18 January 2006
Available online 20 February 2006

Abstract

The NMR structure of the oxidised wild-type cytochrome c_3 from *Desulfovibrio vulgaris* Hildenborough was determined in solution. Using a newly developed methodology, NMR data from the K45Q mutant was then grafted onto data from the wild-type protein to determine the structure in the region of the mutation. The structural origins of the redox-Bohr effect and haem–haem cooperativities are discussed with respect to the redox-related conformational changes observed in solution.

Keywords: Cytochrome c_3; Tetrahaem cytochrome c_3; Multihaem cytochromes; Redox proteins; NMR

1. Introduction

Several multihaem *c*-type cytochromes are found in sulfate-reducing bacteria [1], the most well characterised being the cytochromes c_3. Many of these cytochromes c_3 are small tetrahaem electron-transfer proteins; they receive electrons and protons generated by the oxidation of molecular hydrogen by an hydrogenase [2] and donate the electrons to the electron-transfer chain to be used for the reduction of sulfate, releasing activated protons that can be used by ATP synthase to generate ATP [3].

Tetrahaem cytochromes c_3 have the *c*-type haem groups joined to the polypeptide chain by thioether linkages provided by cysteinyl residues, with two histidinyl residues as the axial ligands of each iron. The haem binding sites along the polypeptide chain have a conserved sequence of the type –C–X–X–(X)–(X)–C–H– where the histidinyl residue following the second cysteinyl residue acts as the fifth iron ligand, the first four being the pyrrole nitrogens of the haem cofactor. The four haem groups are low-spin and are structurally and functionally non-equivalent, with different negative reduction potentials [4]. Despite the low amino acid sequence identity between tetrahaem cytochromes c_3 from different organisms (which include fewer than a dozen residues apart from those responsible for the binding of the haems), and the differences they exhibit in properties such as the isoelectric point and the reduction potential of the individual haems, the available three-dimensional structures have shown that the architecture of the haems and the general fold of the polypeptide chain are conserved [5,6].

Abbreviations: lovs, lower volume limits; upvs, upper volume limits

* Corresponding author. Instituto de Tecnologia Química e Biológica, Universidade Nova de Lisboa, Rua da Quinta Grande 6, 2780-156 Oeiras, Portugal. Tel.: +351 214469821; fax: +351 214428766.
E-mail address: turner@itqb.unl.pt (D.L. Turner).
[1] Present address: European Molecular Biology Laboratory, Structural and Computational Biology Programme, Meyerhofstraße 1, 69117 Heidelberg, Germany.

0005-2728/$ - see front matter © 2006 Elsevier B.V. All rights reserved.
doi:10.1016/j.bbabio.2006.01.007

The tetrahaem cytochrome c_3 from *Desulfovibrio vulgaris* was the first to be isolated and its discovery was reported independently by two groups in 1954 [7,8]. It has been shown that the microscopic haem midpoint reduction potentials of this protein depend on the redox state of the other haems [9–12] and also on the pH [10–12]. These properties have been rationalised in terms of homotropic (electron/electron) and heterotropic (electron/proton) cooperativities [10,12], largely due to electrostatic interactions. However, there is a significant positive cooperativity between the two intermediate haems to be oxidised, haems I and II, which cannot be explained by direct electrostatics. Instead, this implies a redox-linked conformational change in the region of the two haems [13]. Analysis of the pH effect on the redox potentials (the redox-Bohr effect) showed that the heterotropic cooperativities are all positive, with pK_a values increasing along the reduction process (macroscopic pK_a values of 5.3, 5.6, 6.4, 7.1, and 7.4 for fully oxidised, one-, two-, three-, and four-electron-reduced proteins, respectively [11]). This pH dependence is mediated by ionisable groups close to haem I, which has the most strongly pH dependent reduction potential [10,14]. It was concluded that: (i) up to two protons participate in the redox-Bohr effect [3]; (ii) the cytochrome has the ability to couple proton transfer with a concerted two-electron transfer [10]. Thus, it is important to understand the thermodynamic properties of this cytochrome at the molecular level, to identify the groups responsible for the homotropic and heterotropic cooperativities and to rationalise their role in these phenomena. It is therefore appropriate to carry out structural studies, particularly in solution.

A three-dimensional structure for fully oxidised cytochrome c_3 from *Desulfovibrio vulgaris* (Hildenborough) was determined using X-ray crystallography [5,15] and a solution structure for the fully reduced form was obtained using NMR [16]. The structural basis for the pH dependence of the redox potential has also been investigated by site-directed mutagenesis of charged residues in the vicinity of haem I [14]. In particular, Lys 45, which is located in the neighbourhood of the propionates of haem I, was replaced by glutamine. The thermodynamic properties of the mutated cytochrome pointed to a functional role of Lys 45 in the control of the pK_a of the propionate groups of haem I and to its involvement in the redox-Bohr effect as well in the positive haem–haem cooperativity [14]. In another study, Thr 24, located in the vicinity of haem III, was replaced by valine in order to probe the effect of hydrogen-bond networks in controlling reduction potentials [17].

We report here the determination of the NMR structures of the wild-type and K45Q ferricytochromes c_3 from *Desulfovibrio vulgaris* (Hildenborough) [18]. The proton spectrum of the oxidised wild-type protein was almost fully assigned and, although the amount of K45Q mutant was much smaller than that of the wild-type protein, resulting in spectra of poorer quality, it was still possible to assign and measure a significant number of proton–proton NOEs. A form of grafting was used to determine the structure for the mutant protein in the vicinity of the changed residue, a procedure which was designed to maximise efficiency as well as local precision. Selected NOESY peaks from the mutant were used to replace volumes used for the calculation of the structure of the wild-type protein, as described in the experimental part. This novel grafting procedure, which is applicable in the case of verifiably localised structural changes, not only reduces the time spent in the procedure of integration, but also allows the use of more constraints in situations where the quality of the spectra is poor.

2. Experimental procedures

2.1. Sample preparation

2.1.1. Wild-type protein

Cytochrome c_3 from *Desulfovibrio vulgaris* Hildenborough was purified as described [18] then dialysed at 4 °C, first against 0.1 M NaCl to remove residual buffer, and then against deionised water (Millipore). The sample was filtered using a Millex-GS filter unit with 0.22 μm pore size and then lyophilised. For NMR experiments in H_2O the protein was dissolved in 92% H_2O/8% ^2H_2O. For NMR experiments in ^2H_2O the protein was lyophilised four times from ^2H_2O, incubated at 321 K for 2 h and lyophilised again, then dissolved in ^2H_2O (99.98 atom%). An antibiotic cocktail (127 μM ampicillin, 78 μM kanamicin, 141 μM chloramphenicol) was added in order to prevent bacterial growth. The pH was monitored using a glass electrode (Ingold) inserted directly in the NMR tube and the value was adjusted to 7.1 (direct meter reading without correction for the isotope effect [19]). The final protein concentration was approximately 2.7 mM.

2.1.2. K45Q protein

Site-directed mutagenesis and purification of the mutated protein was performed as previously described [14,20]. The rest of the sample preparation was similar to that for the wild-type protein. Due to the small amount of protein available, the final concentration of protein was rather low, approximately 0.85 mM, and no sample in ^2H_2O was prepared.

2.2. NMR spectroscopy

^{1}H-NMR spectra were obtained with a Bruker DRX-500 spectrometer equipped with a 5-mm inverse detection probe with an internal B_o gradient coil. The sample temperature was controlled using a Eurotherm 818 temperature control unit with a B-CU 05 cooling unit.

Assignments were made using spectra acquired at 303 K but additional spectra were obtained at 307 K to help resolve peak overlap. All 2D spectra were acquired in the phase sensitive mode by the States-TPPI method [21] collecting 4096 (t_2) × 1024 (t_1) data points with at least 40 scans per increment. NOESY spectra [22,23] were recorded with 20 ms (spectral widths of 11 and 27.5 kHz) and 80 ms mixing times. The short mixing time spectra were used for the analysis of the resonances from the haem and the haem ligands as well as for some protons very close to haems. Spectra with the larger spectral width were used for the investigation of the most shifted resonances, while the others were used for the study of the crowded regions in order to have better resolution. NOESY spectra of the ^2H_2O sample were recorded with standard pulse sequences with continuous low-power water presaturation during the relaxation delay (0.4 to 0.5 s) and the mixing time. NOESY spectra of the H_2O sample were recorded similarly for the larger spectral width, but with water suppression using the WATERGATE sequence [24] for the smaller spectral width. In that case, presaturation of the water resonance by a composite 180° pulse was followed by a SCUBA sequence to facilitate recovery of potentially saturated α protons [25]. Total correlation spectra were acquired using the clean TOCSY pulse sequence [26–28] with spin-lock times of 20 and 40 or 50 ms for a spectral width of 17 kHz, and with spin-lock time of 75 ms for a spectral width of 12 kHz. COSY [21,29] and DQF-COSY [30,31] spectra were also recorded with a spectral width of 17 kHz. Raw data were multiplied in the F_2 dimension by a function with line narrowing of 5 Hz and Gaussian broadening of 0.05, and by a pure cosine-squared function in the F_1 dimension, except for the COSY spectra, which were multiplied by a pure sine-squared function in both dimensions. The 2D spectra were typically processed to a final size of 4 k × 1 k data points, except COSY spectra, which were processed with 1 k × 1 k data points. Polynomial baseline corrections were applied in both dimensions of

each spectrum. Data were processed using XWINNMR software (Bruker, Rheinstetten). Proton chemical shifts are referenced to the resonances of the methyl groups in DSS at 0.0 p.p.m. using water as the internal reference (at 4.70 p.p.m.).

2.3. Assignment and integration

2.3.1. Assignment of the wild-type protein

The software package XEASY (version 1.2; ETH, Zürich) [32] was used to display and annotate spectra and for volume integration of NOESY cross-peaks. Amino acid residue assignment was performed using the classical approach described by Wüthrich [33]. Examination of the TOCSY and COSY spectra in ^2H_2O and H_2O at two different temperatures allowed the identification of the spin-systems. Analysis of the NOESY spectra and identification of H^N–H^N, H^N–Hα and H^N–Hβ connectivities between different spin-systems allowed the sequential assignment. At later stages of the assignment procedure, approximate pseudocontact shifts were obtained by subtraction of the chemical shifts in the reduced state [16] from those of the same protons in the oxidised state and were used to calculate an empirical magnetic tensor with respect to the X-ray crystal structure [15]. The predicted dipolar shifts were used as a guide for further assignment [34] and were also helpful for the elimination of misassignments. Stereospecific assignments were obtained in the process of structure calculation using the program GLOMSA [35].

2.3.2. Assignment of the K45Q protein

Spectra for the K45Q protein were compared with the corresponding spectra for the wild-type protein. For many spin-systems, it was possible to arrive at the assignment by simple comparison since the chemical shifts differed by less than 0.1 p.p.m. for the two proteins. The assignment procedure for the remaining signals was the same as that followed for the wild-type protein.

2.3.3. Integration of the spectra

Integration was performed manually for isolated peaks and with line-shape integration for overlapped peaks. The baseline around each individual peak or cluster of peaks was determined and used to correct the volume. NOESY cross peaks involving protons at fixed distances and pairs of protons belonging to the same haem (except those of the haem propionates) were not integrated. In the case of the K45Q protein, only selected peaks were integrated, as described below.

2.4. Determination of restraints

2.4.1. Distance restraints

Volumes of NOESY cross-peaks that involved exchangeable protons in the spectra of the H_2O samples were corrected for the percentage of ^2H_2O present. For the wild-type protein, signals involving α protons close to the H_2O frequency were taken from the ^2H_2O spectra, except for the H^N–Hα cross-peaks. NOE volumes from cross-peaks involving non-exchangeable protons were integrated both in H_2O and ^2H_2O spectra and used to obtain a scaling factor relating the two spectra [16]; the volumes were then combined into a single dataset. Many cross-peaks that were visible in the 20-ms NOESY spectra disappear or are less intense at 80 ms because of paramagnetic relaxation. Therefore, for the first (preliminary) structure calculations, all cross-peaks involving haem groups and haem ligands were measured from the 20 ms spectra. A separate calibration was used for the two mixing times and scaling factors were determined for spectra of samples in H_2O and ^2H_2O, obtained at both 20 ms and 80 ms mixing times, and, in the case of 20 ms, with large and small spectral widths. Instead of integrating every peak in spectra for both mixing times, the cross-peak volumes were calculated with respect to the preliminary structures using complete relaxation matrix analysis [36–38]. Peaks with intensities predicted to increase by less than a factor of two between 20 ms and 80 ms were measured at both mixing times and the larger volume was used in each case. In the 80-ms spectra, volumes for non-exchangeable protons were measured in both ^2H_2O and H_2O. A similar process was applied to the spectra measured at 20 ms, both for the large and the small spectral widths. The two sets of integrals (20 ms and 80 ms) were processed separately to convert them into upper and lower volumes using the algorithm described previously and used in the program INDYANA [39]. Before being used in the final structure calculations, these four sets of values (20 ms and 80 ms, upper and lower volumes) were corrected for reduction of the NOE intensities by electron-nuclear dipolar relaxation caused by the paramagnetic haem groups [40].

2.4.2. Angle restraints

It has been shown that in a bishistidinyl ligated haem the orientation of the two histidines can be obtained from the ^{13}C Fermi contact shifts of the haem substituents [41,42]. Angle restraints were used to define the histidine ring orientations for each of the four haems of the wild-type protein within ranges of ±15° for haems I, II and IV and ±20° for haem III [34]. For the K45Q protein, angle restraints were used only for haems III and IV.

2.4.3. Dipolar shifts as restraints

Dipolar (pseudocontact) shifts depend on the position of the nucleus relative to the paramagnetic centres and their magnetic axes, hence they are useful for structure determination and refinement for paramagnetic proteins [34]. Simultaneous calculation of the structure and the magnetic susceptibility tensors to fit dipolar shifts was implemented with the program PARADYANA [44].

Approximate dipolar shifts were obtained by subtracting the chemical shifts obtained for the reduced protein [16] from those of the oxidised protein. Although the spectra were obtained at different values of pH (8.5 and 7.1 for the reduced and oxidised forms, respectively), both values exceed the pK_a associated with the redox-Bohr effect by more than one unit (7.4 and 5.3 for the reduced and oxidised forms, respectively) and no protonation effects on the chemical shifts are expected to occur between pH 7.1 and 8.5, with the possible exception of the N-terminal residue. To allow for possible redox related changes in the hydrogen bonding network, H^N chemical shifts were not used. The shifts of non-specifically assigned diastereotopic pairs of protons were also removed (except when the values for both protons of the pair differ by less than 0.2 p.p.m.), as well as shifts for Hα or for protons belonging to side-chains where differences between calculated and experimental dipolar shifts larger than 0.5 p.p.m. were detected. In residues with a side-chain proton showing an anomalous dipolar shift, the shifts of all protons further from the backbone were also excluded. The remaining dipolar shifts were used to fit the magnetic susceptibility tensor parameters to the coordinates of a preliminary set of twenty structures obtained without the use of dipolar shifts [43], with the uncertainty for the dipolar shifts set to ±0.2 p.p.m. and the uncertainty for the atomic coordinates set to ±0.25 Å. Those dipolar shifts which were not accommodated by these uncertainties in more than ten out of the twenty structures were rejected. These precautions were taken to ensure that the use of dipolar shifts would not prejudice the detection of any structural change between the oxidised and the reduced forms. In computing target functions and gradients, a deviation of 1 p.p.m. in a dipolar shift was treated as equal to a deviation of 1 Å in a distance restraint.

2.4.4. Additional restraints

Four non-standard residues were used for structure calculations: flexible haem macrocycles and proline residues with fixed upper limit distances for ring closure [16,39,46], and fast-flipping Phe and Tyr rings with pseudo-atoms to limit the orientations of their planes [16,44,45]. In addition, two types of histidine axial ligands were defined to take into account the iron–nitrogen bond [16,46], the magnetic axes [46] and the torsion angle that defines the orientation of the histidine ring plane with respect to the haem plane [39].

In the final stages of structure refinement, the calculated structures were checked for short distances (less than 2.5 Å) between assigned protons that should give rise to significant NOEs. The volume at the predicted frequencies was measured if no visible peaks appeared in that region of the spectrum (NOESY spectrum with mixing time of 80 ms and sample in H_2O) and used in further calculations. This procedure provided upvs that ensure that protons will not be allowed to approach each other in the structures if there is no corresponding NOE in the spectrum.

2.5. Structure calculation

The final structures were calculated with the program PARADYANA [46], which was used for the determination of the solution structure of the oxidised

cytochrome c_3 from *Desulfovibrio gigas* [40]. The program uses corrected NOE volumes, angle restraints and dipolar shifts, as described above, and optimises magnetic susceptibility tensors together with the parameters of the structure. After conjugate gradient minimisation to remove strong overlaps, the structures were annealed with 40,000 steps and a weight of 0.1 for the valid dipolar shifts. The weighting of the dipolar shifts was then increased to 0.5 and a further 40,000 steps of annealing were carried out. The weighting of the van der Waals repulsion was then increased to 2.0, followed by conjugate gradient minimisation and 200 steps of molecular dynamics at constant temperature, and a final 2,000 steps of conjugate gradient minimisation.

2.6. Structure analysis

The program MOLMOL (version 2.6) [47] was used for superimposition, visual inspection and calculation of a mean structure and of root-mean-square deviations from the mean structure. It was also used for calculation of solvent accessible surfaces using a radius of 1.4 Å for the H_2O molecule. Stereochemical analysis of the structures was performed with the program PROCHECK-NMR (version 3.4.4) [48]. The program WHAT IF [49] was used for the identification of possible hydrogen bonds in the family of conformers. Identification and classification of the consensus secondary structure elements in the NMR structures ensemble, defined as those present in at least 50% of the structures, were accomplished with the program PROMOTIF (version 2.0) [50].

3. Results

3.1. Sequential assignment

3.1.1. Wild-type protein

Sequential connectivities involving H^N, Hα and Hβ protons are shown in Fig. 1. Unambiguous sequence-specific assignment was obtained for large segments of the sequence: residues 1–37, 39–56, 58–59, 61–72, 74–78 and 80–107. In these segments, all the residues except the prolines (residues 2, 5, 17 and 36) show at least one of the sequential connectivities between its H^N and the H^N, Hα or Hβ of the preceding residue. For proline residues, connectivities were observed at least between the Pro H^δ and the Hα or the Hβ of the preceding residue.

Fig. 1. Sequential NOE connectivities involving H^N, Hα and Hβ in ferricytochrome c_3 from *D. vulgaris* Hildenborough. The line thickness is indicative of the NOE intensity.

Asn 38 exhibits NOEs only to the methyl groups of Val 37, and the sequential NOEs between the pairs of residues 56/57 and 59/60 are probably overlapped with others. The Asn 73 H^N was not assigned but various connectivities were observed between other protons of this residue and Lys 72. The Cys 79 H^N resonance overlaps with the water signal. About 80% of the haem resonances and a few amino acid resonances had been assigned previously [34], and the remainder are now assigned. Some difference from the published values is expected in view of the different experimental conditions (pH values of 5.0 and 9.0; temperatures of 311.5 K and 323 K), but the patterns of signals are in full agreement. The chemical shifts of the axial histidine residues [34] are also specifically assigned. The axial histidine ring resonances are generally broad and only His 52 $H^{\delta 1}$ was assigned specifically.

In total, 86% of the protons in the protein were assigned, which corresponds to 94% of the protons after excluding exchangeable protons other than backbone H^N protons. The chemical shifts have been deposited in the BioMagResBank database (http://www.bmrb.wisc.edu) under accession number BMRB - 5625.

3.1.2. K45Q protein

Due to the low signal-to-noise ratio of the spectra, signals were not assigned for residues 5, 27, and 39. For the mutated residue, Gln 45, one of the γ protons was not found. Most of the chemical shifts are very similar to those for the wild-type protein; differences larger than 0.1 p.p.m. were found for resonances of some protons in the vicinity of residue 45 and for some residues belonging to the N-terminal region. The chemical shifts have been deposited in the BioMagResBank database under accession number BMRB-6634.

3.2. Restraints and calculation of the structures

3.2.1. Wild-type protein

Assigned cross-peaks in the H_2O and the ^2H_2O NOESY spectra were integrated and converted into volume restraints, resulting in 800 lovs and 1620 upvs obtained from the 80 ms NOESY spectra, and 545 lovs and 687 upvs obtained from the 20-ms spectra. These were used together with 8 angle restraints (for the histidine axial ligands) [34] and a set of 124 fixed upper limit distances (associated with the flexible proline residues and haem groups, and with the His ligands [16,39,46]) as input for the program PARADYANA. Initial structures generated without any correction for paramagnetic leakage were used as input for the relaxation matrix calculations. Correction factors were obtained and used to modify each upper and lower volume. The program GLOMSA [35] was used to analyse the structures and to allow stereospecific assignments, which were made for 58 pairs of diastereotopic protons or methyl groups. After adjustment for non-stereospecifically assigned protons, 1284 lovs and 1993 upvs from the 80-ms NOESY spectra and 891 lovs and 863 upvs from the 20-ms NOESY spectra were generated by PARADYANA. This program has the functionality of DYANA [35] and, in addition, optimises the calibration of distance restraints separately for each structure by treating the scaling factors as parameters in parallel with the torsion angles, as well as fitting dipolar shifts. In this case, 238 dipolar shifts were used. For the final stage of structure calculation, structures calculated with the corrected volumes were used as input for relaxation matrix calculations in order to estimate the errors caused by spin diffusion. Corrected distances were obtained which exceeded the range of experimental restraints with an rmsd of 7.6% for the 80 ms data and 7.7% for the 20 ms data. These values were used to soften all distance restraints.

Since the calibration of NOE volumes is fully automatic, restraints that are redundant with respect to distance limits imposed by covalent geometry cannot be identified until the calculation is complete. Therefore, the NOE restraints obtained after adjustment for non-stereospecifically assigned protons were analysed after conversion into distances using the scaling factors of the best structure: the non-redundant distance restraints selected using the program DYANA [35] are summarised in Table 1 of the supplementary material and the number of restraints per residue is shown in Fig. 2. Table 2 of the supplementary material shows a summary of the scaling factors used in the calculation of the structures, the DYANA target function values obtained and the associated restraint violations.

3.2.2. K45Q protein

In view of the four porphyrins in the protein and the effect of four paramagnetic centres, the small differences in chemical shift between the mutant and wild-type proteins indicates that there are no significant conformational changes beyond the immediate vicinity of the mutated residue, Gln 45. Consequently, rather than obtain a low-resolution structure of the complete mutant protein, we sought to define the structure in the region of the mutation more precisely by using data from the wild-type protein to provide a matrix. The modified region was chosen on the basis of NOE effects observed in the wild-type protein involving protons of Lys 45 and protons of other residues, and NOEs from these other residues to the next shell. NOEs were observed connecting Lys 45 with Arg 44, Cys 46,

Table 1
Average iron–iron distances (in Å) in the NMR and X-ray structures

	I–II	I–III	I–IV	II–III	II–IV	III–IV
NMR oxidised	12.85 (0.04)	11.96 (0.11)	17.91 (0.11)	16.70 (0.06)	15.82 (0.09)	11.76 (0.10)
X-ray A	12.41	11.12	17.81	16.04	16.61	11.99
X-ray B	12.36	11.09	17.80	16.20	16.63	12.02
NMR reduced	11.87 (0.05)	10.81 (0.03)	17.57 (0.07)	15.33 (0.03)	15.79 (0.05)	11.97 (0.05)

Values in parentheses correspond to the standard deviation for the family of 20 NMR conformers.

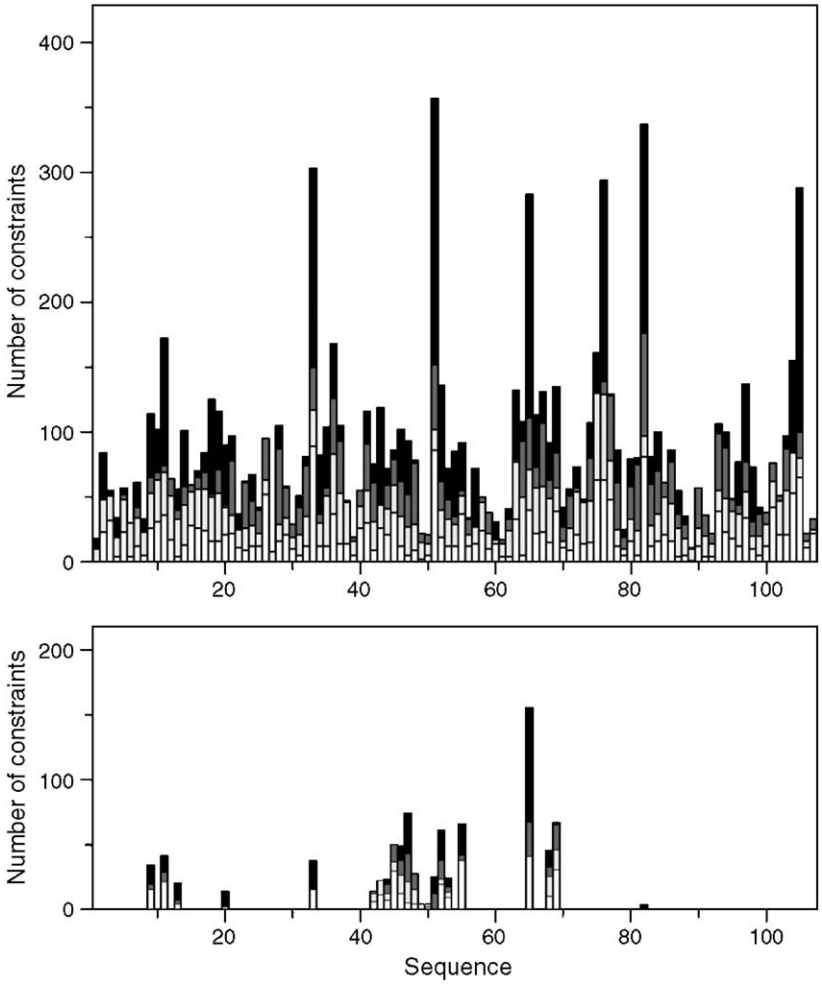

Fig. 2. Number of restraints per residue used for the calculation of the structure of ferricytochrome c_3 from *D. vulgaris* Hildenborough (upper panel) and for the graft used for the K45Q mutant (lower panel). Bars are white, light grey, dark grey and black for intra residue, sequential, medium and long range restraints, respectively. Residues 33, 51, 82 and 105 also include restraints to haems I, II, III and IV, respectively.

Gly 47 and Thr 48 as well as propionate 13 of haem I. Since the haem occupies a large volume, only one quarter of this group was considered to be in the direct vicinity of Lys 45. There were also NOEs for pairs of protons involving residues 44, 46 and 48 to different parts of haem II and, as with haem I, only a part (two quarters) of haem II was considered. Altogether, the following residues were selected as forming the region potentially affected by the alteration of residue 45: 9, 11, 13, 20, pyrrole D of haem I, including HBM and HGM, 42–53, pyrroles B and C of haem II, including HAM, HBM and HDM, 55, 65, 68–69 and pyrrole B of haem III. This represents a total of 22 residues out of 107, which corresponds to about 20% of the protein.

The 80-ms NOESY spectrum of the K45Q mutant yielded 73 lovs and 144 upvs for proton pairs within the selected region. A further 55 lovs and 65 upvs were obtained from the 20 ms spectra in this region. These were added to a set of 677 lovs and 1397 upvs obtained from the 80 ms spectra and 396 lovs and 503 upvs obtained from the 20-ms spectra for the wild-type protein *outside* the selected region. The calculation of structures was performed as described above for the wild-type protein but using only 4 angle restraints and 222 dipolar shifts. The softening factors used to allow for spin diffusion were 6.9% for both the 80-ms and 20-ms data sets. Stereospecific assignments were used for 45 pairs of diastereotopic protons or methyl groups; they were a part of the set taken from the wild-type protein. Detailed data concerning the structure calculation are presented in Tables 1 and 2 of the supplementary material and in Fig. 2.

3.3. Analysis of structures

3.3.1. Wild-type protein

The final family consists of 20 structures with the target function increasing by 15% from the first to the last. The structures have been deposited in the Protein Data Bank under accession number 2BPN. The structures superimpose with an average backbone rmsd of 0.46 Å and a heavy atom rmsd of 0.79 Å with respect to the mean structure; the values for each residue are shown in Fig. 3 and the superimposed structures are shown in Fig. 4. The Ramachandran plot shows 58.9% of the residues in the most favoured regions, 36.2% in the additionally allowed, 3.4% in the generously allowed, and 1.6% in the disallowed regions. The disallowed conformations are primarily

Table 2
Distances (in Å) between some charged residues and the iron of haems I and II

	Oxidised	Reduced
Lys 40 NZ–Haem I Fe	16.18 (0.28)	16.05 (0.28)
Lys 40 NZ–Haem II Fe	15.48 (0.27)	12.69 (0.31)
Lys 40 NZ–Asp 42 OD*	8.23 (0.36)	7.20 (0.41)
Asp 42 OD*–Haem II Fe	8.30 (0.18)	12.20 (0.43)
Asp 42 OD*–Arg 44 NE	4.02 (0.19)	5.45 (0.35)
Arg 44 NE–Haem I O*A	10.03 (0.28)	8.09 (0.25)
Arg 44 NE–Haem I O*D	11.89 (0.80)	11.84 (0.15)
Arg 44 NE–Haem I Fe	13.00 (0.03)	11.78 (0.10)
Arg 44 NE–Haem II Fe	11.29 (0.06)	11.69 (0.19)
Lys 45 NZ–Haem I Fe	13.23 (0.23)	10.73 (0.13)
Lys 45 NZ–Haem II Fe	14.57 (0.15)	14.66 (0.05)
Lys 45 NZ–Haem I O*A	9.64 (0.32)	5.08 (0.24)
Lys 45 NZ–Haem I O*D	7.53 (0.28)	8.43 (0.16)
Haem I O*A–Haem I Fe	8.10 (0.05)	8.32 (0.09)
Haem I O*D–Haem I Fe	8.27 (0.18)	8.45 (0.13)
Haem I O*A–Haem II Fe	16.25 (0.20)	15.35 (0.15)
Haem I O*D–Haem II Fe	10.97 (0.25)	10.04 (0.22)
Lys 75 NZ–Haem II Fe	12.20 (0.31)	10.54 (0.20)
Haem II O*A–Haem II Fe	8.16 (0.15)	8.48 (0.07)
Haem II O*D–Haem II Fe	7.92 (0.18)	8.23 (0.08)
Lys 75 NZ–Haem II O*A	8.49 (0.23)	8.58 (0.28)
Lys 75 NZ–Haem II O*D	8.48 (0.33)	8.60 (0.28)

Values in parentheses correspond to the standard error for the family of 20 NMR conformers.

due to Thr 48. In fact both Gly 47 and Thr 48 show significantly reduced order parameters. A total of 90 hydrogen bonds was identified in the family of 20 structures with the program WHAT IF (using routine HBO) [49], 31 of which were present in at least 50% of the structures. Backbone torsion angles, Φ and Ψ, with values for the order parameter, S, larger than 0.8 are observed for residues 5–25, 28–36, 39–59, 62–86 and 89–107. In the portion of the backbone containing residues 39 to 59, the mean values for S were 0.978 for Φ and 0.982 for Ψ; the only values of S smaller than 0.9 were those for Ψ of Gly 47 (0.826) and for Φ of Thr 48 (0.815). The structure contains several elements of regular secondary structure, in particular two short β-chains forming a two-stranded antiparallel β-sheet (Leu 9–Met 11 and Val 18–Phe 20), two α-helices (Lys 29–His 34 and Cys 79–Ala 87) and two short 3_{10}-helices (His 21–Lys 26 and Ala 92–Asp 96). The less well-defined regions of the NMR structure generally correlate with high solvent exposure.

3.3.2. K45Q protein

The final family consists of 20 structures with the target function increasing by 14% from the first to the last. The structures superimpose with an average backbone rmsd of 0.58 Å and a heavy atom rmsd of 0.95 Å to the mean structure; the values for each residue are shown in Fig. 3 and the superimposed structures are shown in Fig. 4. The Ramachandran plot shows 57.7% of the residues in the most favoured regions, 34.9% in the additionally allowed, 5.8% in the generously allowed and 1.5% in the disallowed regions. The disallowed conformations were due not only to Thr 48, as in the wild-type, but also to Ser 27, Arg 44 and Ser 61 in some of the structures. A total of 104 hydrogen bonds was identified in the family of 20 structures with the program WHAT IF (routine HBO) [49], 30 of which were present in at least 50% of the structures. The NMR structure of the mutant is not as well defined as the one for the wild-type protein, with order parameters for the backbone torsion angles Φ and Ψ smaller than 0.8 in the same regions as for the wild-type protein, but also for residues 21, 44–45 and 48–50. Low values for the order parameter S were found for, among others, Φ of Ser 27 (0.380), Φ of Arg 44 (0.693), Ψ of Arg 44 (0.591), Ψ of Thr 48 (0.666) and Φ of Ser 61 (0.273). The structures also contain several elements of regular secondary structure, in particular two β-chains forming a two-stranded antiparallel β-sheet (Leu 9–Met 11 and Val 18–Phe 20), three α-helices (Lys 29–His 34, Gly 64–Met 69 and Ser 78–Ala 87) and two 3_{10}-helices (His 22–Lys 26 and Ala 92–Asp 96).

4. Discussion

4.1. Comparison of the NMR and X-ray structures of the oxidised wild-type protein

The solution NMR structure of the wild-type protein was compared with the available X-ray structures [5] for *Desulfovibrio vulgaris* Hildenborough cytochrome c_3 in the oxidised form. The general fold and the relative position of the four haems are similar, and there is good agreement between some of the consensus secondary structure elements identified in the NMR and the X-ray structures. A two-stranded antiparallel β-

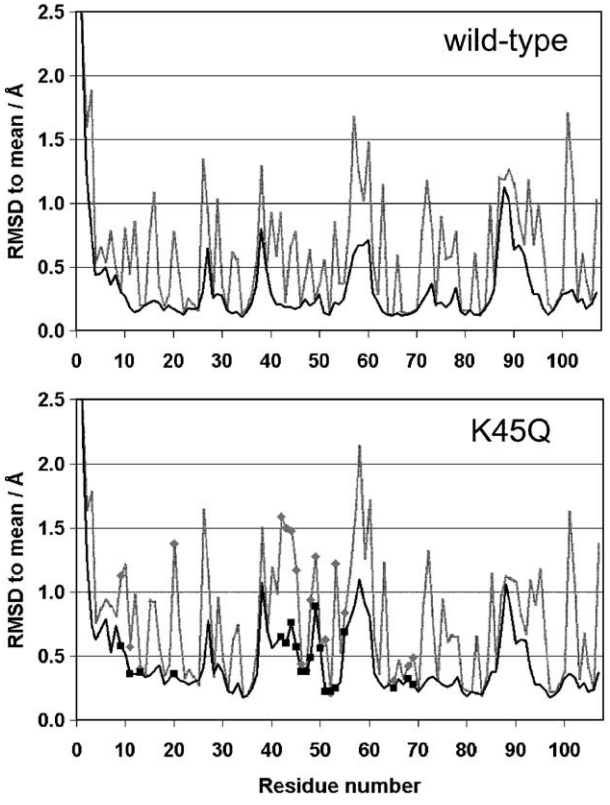

Fig. 3. Average backbone and heavy atom rmsd values per residue with respect to the mean structure of the family of 20 conformers obtained for ferricytochrome c_3 from *D. vulgaris* Hildenborough and its K45Q mutant. In the case of the mutant, residues that form part of the graft are picked out with solid symbols.

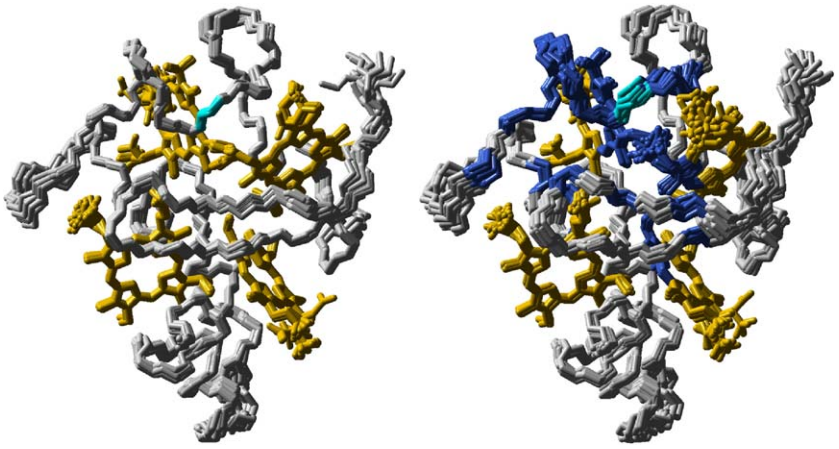

Fig. 4. The backbone and haems from the NMR structures of the wild-type (left) and K45Q (right) ferricytochrome c_3 from *D. vulgaris* Hildenborough. The calculation of the K45Q structure was performed with data from regions coloured blue grafted onto data from the wild-type protein. Gln 45, the mutated residue, is shown in cyan. The N-terminus is at the top-right, near haem I; haems III, IV, and I appear clockwise. The figure was produced using Molmol [47].

sheet (Leu 9–Met 11 and Val 18–Phe 20) is found in both structures, but a second one of similar size is present only in the X-ray structure (His 35–Val 37 and Lys 40–Gln 42). The X-ray structure contains three α-helices (Tyr 65–His 70, Cys 79–Ala 87 and Ala 91–Thr 98): the first does not appear in the solution structure, the second (Cys 79–Ala 87) is exactly coincident with one of the α-helices of the NMR structure, and the third becomes a 3_{10}-helix in the NMR structure (Ala 92–Asp 96).

The average iron–iron distances found in the NMR and X-ray structures differ by less than 5%, except for the distance between the irons of haems I and III which is 8% larger in the NMR structure (Table 1). The global rmsd values of the mean NMR structure to molecule A and molecule B of the unit cell of the crystal are 1.16 Å and 1.14 Å for the backbone and 1.71 Å and 1.69 Å for all heavy atoms, respectively. These values are only slightly higher than those found for the two molecules in the unit cell of the crystal, which are 0.92 Å and 1.18 Å for the backbone and all heavy atoms, respectively.

4.2. Comparison of the NMR structures of the oxidised and reduced wild-type protein

In order to focus on redox-dependent conformational changes, the solution pH values of both the oxidised and the reduced [16] samples were set more than 1 pH unit higher than their redox-Bohr pK_a values, ensuring that the ionisable centres involved in the redox-Bohr effect are essentially deprotonated in both states. Therefore, any conformational changes detected are only dependent on the oxidation state.

The general fold of the solution structures for the reduced and oxidised proteins is very similar and there are only small differences between the consensus secondary structure elements. The two-stranded antiparallel β-sheet (Leu 9–Met 11 and Val 18–Phe 20) was found in both oxidation states, as well as one of the α-helices (Lys 29–His 34). The other α-helix (Ser 78–Gly 88 in the reduced form) involves two fewer residues (Cys 79–Ala 87) in the oxidised form. A third α-helix in the reduced form (Ala 92–Lys 94) is found in approximately the same position as a 3_{10}-helix in the oxidised form (Ala 92–Asp 96). Another 3_{10}-helix (His 22–Lys 26) in the oxidised form corresponds to a composite β-turn in the reduced form and a 3_{10}-helix in the reduced form (Gly 64–Val 68) was not found in the oxidised form. The relative arrangement of the four haems is similar and the average iron–iron distances differ at most by 10% (Table 1), tending to be larger in the oxidised protein. Thus, it appears that a slight expansion accompanies oxidation of the protein. The global rmsd values between the mean NMR structures are 1.22 Å and 1.59 Å for the backbone and all heavy atoms, respectively, which are similar to those obtained for the X-ray and the NMR structures of the oxidised protein.

A remarkable difference in the two structures is found in the region of Thr 24. A different orientation of the side-chain of this residue allows the formation of two hydrogen bonds (Thr 24 HN to Thr 24 OG1 distance 2.24 (0.09) Å and Thr 24 OG1 to His 25 HD1 2.19 (0.18) Å, with standard deviations for the family of 20 NMR conformers in parentheses) in the oxidised protein but none in the reduced protein [16]. Thus, the reduced form is destabilised by the loss of two hydrogen bonds, one of them involving His 25, an axial ligand of haem III.

4.3. Comparison of the NMR structures of the oxidised wild-type and K45Q proteins

The structures obtained for the wild-type and K45Q proteins in the fully oxidised state are very similar, the global rmsd values between the mean structures being 0.65 Å and 0.89 Å for the backbone and all heavy atoms, respectively. These values are not too different from the values of 0.46 Å and 0.79 Å obtained for the average backbone and heavy atoms, respectively, of the family of 20 structures for the wild-type protein. However, because of the methodology, only the structure in the region of the mutation can meaningfully be discussed. The close similarity in chemical shifts of the wild type and mutant proteins led us to conclude that the structure is unperturbed outside the immediate vicinity of the site of mutation. Consequently, only NOEs involving 20 residues (and four haem pyrroles) that have

NOEs with residue 45 or its nearest neighbours were measured in spectra of the mutant (see Fig. 4). Thus, the bulk of the structure is determined by well-defined NOEs from the wild-type protein, providing a framework with some flexibility at the interface, and the region of the mutation is grafted on to this. This procedure ensured that the definition of the local structural modifications is not severely degraded by the poor signal to noise ratio obtained in NOESY spectra of the mutant. The success of the procedure may be judged from the absence of constraint violations in the mutant graft or its interface with the wild-type matrix. Generally, the structure of the grafted region in the mutant is similar to that of the wild-type protein. Interestingly, slight changes in torsion angles lead to a new α-helix appearing in the region Gly 64–Met 69, which is almost coincident with one of the α-helices of the X-ray crystal structure (Tyr 65–His 70). The distances that define the proximity of the backbone of residues 44 to 47 to haem I are similar to those for the wild-type protein, although there is a movement of about 1.0 Å broadly parallel to the vector haem I CAD–haem I CAA.

4.4. Structural basis for positive cooperativity

For two haems to be involved in positive redox cooperativity, the reduction of one haem must facilitate the reduction of the other and, similarly, the oxidation of one haem facilitates the oxidation of the other. The reduction or oxidation of an individual haem is commonly accompanied by some conformational change in the protein or in the haem itself, which acts to stabilise the oxidation state. For positive redox cooperativity to exist, the conformational changes associated with the reduction of one haem must not only stabilise the reduced state of this haem, but also the reduced state of the other haem, either directly or by stabilising the conformational changes that accompany reduction of this second haem. Similar reasoning applies in the direction of oxidation. Therefore, the first step towards unravelling the structural origins of the effect is to identify conformational changes that stabilise each of the haems individually in either of its states. The second step is to distinguish those changes that stabilise both haems simultaneously in the same state.

In the vicinity of haems I and II, the haems involved in positive cooperativity, significant differences are observed between the reduced and the oxidised state for residues 40–47 (see Fig. 5), including a rearrangement of the propionates of haem I (Table 2). The regions of redox-related changes in conformation found by MD simulation are in broad agreement although the computational method is less specific and the largest changes were found for residues 36–42 [51]. There is a coupled movement of Arg 44 and Lys 45 such that the positively charged NE of Arg 44 and NZ of Lys 45 are closer to the iron of haem I in the reduced state. These conformational changes stabilise haem I electrostatically upon reduction or upon oxidation. Movement of Lys 40 and Asp 42 brings the positively charged NZ of Lys 40 closer to the iron of haem II in the reduced state, while the negatively charged carboxyl oxygen atoms of Asp 42 become significantly more distant from it

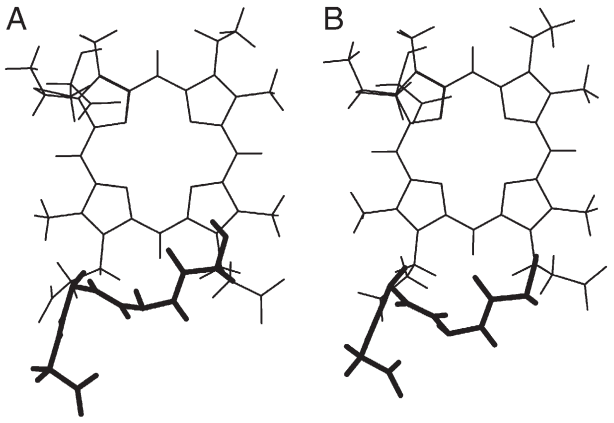

Fig. 5. Relative position of haem I and the backbone of the polypeptide chain (residues 44–47) for the best NMR structure (A) of ferrocytochrome c_3 [15] and (B) of ferricytochrome c_3 from *D. vulgaris* Hildenborough.

(Table 2). The rearrangements also result in the charged oxygen atoms of Asp 42 moving further from the NE of Arg 44 and approaching Lys 40 NZ upon reduction.

There is also a rearrangement of Lys 75 such that Lys 75 NZ is closer to the iron of haem II when it is reduced (Table 2). The conformation of both propionates changes such that the distances between their charged groups and Lys 75 NZ change only marginally between the two oxidation states. However, the conformational change for Lys 75 appears to affect only haem II and so does not appear to be involved in the observed positive cooperativity.

The haem reduction potentials are lower in the K45Q mutant, as expected with the removal of the positively charged lysine, but only in the fully reduced form [14]. There is a slight increase in the reduction potentials of the oxidised and deprotonated form which is largely attributable to a marked reduction in the positive cooperativity between haems I and II, which further emphasises the role of Lys 45. The haem–haem interactions in the mutant are generally weaker than those in the wild-type protein, as though the effective dielectric constant had increased throughout the protein, and yet the interactions with the acid/base group responsible for the redox-Bohr effect all increase. These changes are likely to be associated with a subtle redox-related reorganisation of hydrogen bonds, such as those associated with the rotation of Thr 24 seen in these structures. Indeed, removing the hydroxyl in the T24V mutant increases the interactions of the haems with the acid/base group, and increases the reduction potential of the neighbouring haem III by ca. 80 mV, and that of haem I by ca. 40 mV [17].

4.5. Structural basis for the redox-Bohr effect

Table 2 shows that, on oxidation of the wild-type protein, Lys 45 NZ moves away from propionate 17, getting closer to propionate 13. Although propionate 13 appears in two major different conformations in the oxidised state, Lys 45 NZ is significantly closer to its oxygen atoms in either conformation than it is in the reduced state (Table 2). At pH 7.1, the lysine

amino group and the propionate carboxyl group are positively and negatively charged, respectively. Therefore, the increase of the distance between the charged groups of Lys 45 and propionate 13 in the reduced state should stabilise the protonated form of propionate 13, raising the redox-Bohr pK_a even further than expected on the basis of the change in haem charge.

The K45Q mutation increases the pK_a of the reduced form from 7.4 to 9.3 [14], in the direction expected by eliminating the charge of Lys 45. However, the redox-Bohr pK_a of the fully oxidised K45Q protein is unaltered at 5.3, which correlates with a greater solvent exposure of propionate 13 of haem I in the oxidised mutant. In the reduced form, the exposure is lowered by movement of residues 44–46 towards the interior of the protein [14].

5. Conclusions

Despite their importance, few structures of multicentre paramagnetic proteins have been determined in solution. Although the statistics show that the structures of the oxidised protein are slightly less precise than those of the reduced form, we have shown that it is possible to obtain structures of good quality and, further, to focus on localised changes in mutant proteins when material is scarce.

The structures of *D. vulgaris* cytochrome c_3 have begun to reveal how the affinity for electrons and protons is controlled. Rearrangement of residues in the segment 40–45 stabilises the reduced state of haems I and II upon reduction, and the oxidised state of both haems upon oxidation, thus contributing to the positive cooperativity between the two haems. The charge of Lys 45 is central to the effect, and the conformational change extends as far as Thr 24. The redox-Bohr pK_a is influenced by the charge of the haems but the strength of coupling between electron and proton transfer is increased by a combination of changing solvent exposure and the movement of charged groups.

In view of the uncertainties in solution structures and packing forces in crystals, we would not expect to explain its thermodynamic properties in detail at this stage. With its four redox centres (which undergo fast intramolecular electron transfer) and one ionisable group, this protein may have 10 distinct conformations in its different states. Conformational changes in the protonated, low pH, forms remain to be explored and, crucially, it remains to be determined at which stage of oxidation the redox-related conformational changes occur. Nonetheless, this study has cast light on the structural factors that control the energetics, and this may provide a model for mechanisms that operate in other, more complex, systems.

Acknowledgements

This work was supported by Grant POCTI/2002/QUI/47866 awarded to A. V. Xavier by Fundação para a Ciência e Tecnologia (FCT), Portugal. A. C. Messias acknowledges FCT for a doctoral fellowship (PRAXIS XXI BD/2709/94).

Appendix A. Supplementary data

Supplementary data associated with this article can be found in the online version at doi:10.1016/j.bbabio.2006.01.007.

References

[1] I.A.C. Pereira, M. Teixeira, A.V. Xavier, Hemeproteins in anaerobes, Struct. Bond. 91 (1998) 65–89.
[2] T. Yagi, M. Honya, N. Tamiya, Purification and properties of hydrogenases of different origins, Biochim. Biophys. Acta 153 (1968) 699–705.
[3] R.O. Louro, T. Catarino, C.A. Salgueiro, J. LeGall, A.V. Xavier, Redox-Bohr effect in the tetrahaem cytochrome c_3 from *Desulfovibrio vulgaris*: a model for energy transduction mechanisms, J. Biol. Inorg. Chem. 1 (1996) 34–38.
[4] I.B. Coutinho, A.V. Xavier, Tetraheme cytochromes, Methods Enzymol. 243 (1994) 119–140.
[5] P. Simões, P.M. Matias, J. Morais, K. Wilson, Z. Dauter, M.A. Carrondo, Refinement of the three-dimensional structures of cytochromes c_3 from *Desulfovibrio vulgaris* Hildenborough at 1.67 Å resolution and from *Desulfovibrio desulfuricans* ATCC 27774 at 1.6 Å resolution, Inorg. Chim. Acta 273 (1998) 213–224.
[6] S. Nørager, P. Legrand, L. Pieulle, C. Hatchikian, M. Roth, Crystal structure of the oxidised and reduced acidic cytochrome c_3 from *Desulfovibrio africanus*, J. Mol. Biol. 290 (1999) 881–902.
[7] J.R. Postgate, Presence of cytochrome in an obligate anaerobe, Biochem. J. 58 (1954) xi–xii.
[8] M.K. Ishimoto, J. Koyama, Y. Nagai, A cytochrome and a green pigment of sulfate-reducing bacteria, Bull. Chem. Soc. Jpn. 27 (1954) 564–565.
[9] K. Fan, H. Akutsu, Y. Kyoguku, K. Niki, Estimation of microscopic redox potentials of a tetraheme protein, cytochrome c_3 of *Desulfovibrio vulgaris*, Miyazaki F., and partial assignments of heme groups, Biochemistry 29 (1990) 2257–2263.
[10] D.L. Turner, C.A. Salgueiro, T. Catarino, J. LeGall, A.V. Xavier, Homotropic and heterotropic cooperativity in the tetrahaem cytochrome c_3 from *Desulfovibrio vulgaris*, Biochim. Biophys. Acta 1187 (1994) 232–235.
[11] D.L. Turner, C.A. Salgueiro, T. Catarino, J. LeGall, A.V. Xavier, NMR studies of cooperativity in the tetrahaem cytochrome *c*3 from *Desulfovibrio vulgaris*, Eur. J. Biochem. 241 (1996) 723–731.
[12] C.A. Salgueiro, D.L. Turner, J. LeGall, A.V. Xavier, Reevaluation of the redox and redox-Bohr cooperativity in tetrahaem *Desulfovibrio vulgaris* (Miyazaki F) cytochrome c_3, J. Biol. Inorg. Chem. 2 (1997) 343–349.
[13] H. Santos, J.J.G. Moura, I. Moura, J. LeGall, A.V. Xavier, NMR studies of electron transfer mechanisms in a protein with interacting redox centres: *Desulfovibrio gigas* cytochrome c_3, Eur. J. Biochem. 141 (1984) 283–296.
[14] L.M. Saraiva, C.A. Salgueiro, P.N. da Costa, A.C. Messias, J. LeGall, W. M.A.M. van Dongen, A.V. Xavier, Replacement of lysine 45 by uncharged residues modulates the redox-Bohr effect in tetraheme cytochrome c_3 of *Desulfovibrio vulgaris* (Hildenborough), Biochemistry 37 (1998) 12160–12165.
[15] P.M. Matias, C. Frazão, J. Morais, M. Coll, M.A. Carrondo, Structure analysis of cytochrome c_3 from *Desulfovibrio vulgaris* Hildenborough at 1.9 Å resolution, J. Mol. Biol. 234 (1993) 680–699.
[16] A.C. Messias, D.H.W. Kastrau, H.S. Costa, J. LeGall, D.L. Turner, H. Santos, A.V. Xavier, Solution structure of *Desulfovibrio vulgaris* (Hildenborough) ferrocytochrome c_3: structural basis for functional cooperativity, J. Mol. Biol. 281 (1998) 719–739.
[17] C.A. Salgueiro, P.N. da Costa, D.L. Turner, A.C. Messias, W.M.A.M. van Dongen, L.M. Saraiva, A.V. Xavier, Effect of hydrogen-bond networks in controlling reduction potentials in *Desulfovibrio vulgaris* (Hildenborough) cytochrome c_3 probed by site-specific mutagenesis, Biochemistry 40 (2001) 9709–9716.
[18] R.O. Louro, T. Catarino, D.L. Turner, M.A. Piçarra-Pereira, I. Pacheco, J. LeGall, A.V. Xavier, Functional and mechanistic studies of cytochrome c_3

from *Desulfovibrio gigas*: thermodynamics of a "proton thruster", Biochemistry 37 (1998) 15808–15815.
[19] P.K. Glasoe, F.A. Long, Use of glass electrodes to measure acidities in deuterium oxide, J. Phys. Chem. 64 (1960) 188–191.
[20] L.M. Saraiva, C.A. Salgueiro, J. LeGall, W.M.A.M. van Dongen, A.V. Xavier, Site-directed mutagenesis of a phenylalanine residue strictly conserved in cytochromes c3, J. Biol. Inorg. Chem. 1 (1996) 542–550.
[21] D. Marion, K. Wüthrich, Application of phase sensitive two-dimensional correlated spectroscopy (COSY) for measurement of ^{1}H–^{1}H spin–spin coupling constants in proteins, Biochem. Biophys. Res. Commun. 113 (1983) 967–974.
[22] J. Jeener, B.H. Meier, P. Bachmann, R.R. Ernst, Investigation of exchange processes by two-dimensional n.m.r. spectroscopy, J. Chem. Phys. 71 (1979) 4546–4553.
[23] A. Kumar, G. Wagner, R.R. Ernst, K. Wüthrich, A two-dimensional nuclear Overhauser enhancement (2D NOE) experiment for the elucidation of complete proton–proton cross-relaxation networks in biological macromolecules, Biochem. Biophys. Res. Commun. 95 (1980) 1–6.
[24] M. Piotto, V. Saudek, V. Sklenár, Gradient-tailored excitation for single quantum NMR spectroscopy of aqueous solution, J. Biomol. NMR 2 (1992) 661–665.
[25] S.C. Brown, P.L. Weber, L. Mueller, Towards complete ^{1}H NMR spectra in proteins, J. Magn. Reson. 77 (1988) 166–169.
[26] D.W. Bearden, S. Macura, L.R. Brown, Suppression of cross relaxation in TOCSY experiments on macromolecules, J. Magn. Reson. 80 (1988) 534–538.
[27] C. Griesinger, K. Otting, K. Wüthrich, R.R. Ernst, Clean TOCSY for ^{1}H spin system identification in macromolecules, J. Am. Chem. Soc. 110 (1988) 7870–7872.
[28] J. Briand, R.R. Ernst, Computer-optimized homonuclear TOCSY experiment with suppression of cross relaxation, Chem. Phys. Lett. 185 (1991) 276–285.
[29] W.P. Aue, E. Bartholdi, R.R. Ernst, Two-dimensional spectroscopy. Application to nuclear magnetic resonance, J. Chem. Phys. 64 (1976) 2229–2246.
[30] M. Rance, O.W. Sørensen, G. Bodenhausen, G. Wagner, R.R. Ernst, K. Wüthrich, Improved spectral resolution in COSY ^{1}H NMR spectra of proteins via double quantum filtering, Biochem. Biophys. Res. Commun. 117 (1983) 479–485.
[31] A.E. Derome, M.P. Williamson, Rapid-pulsing artifacts in double-quantum-filtered COSY, J. Magn. Reson. 88 (1990) 177–185.
[32] C. Bartels, T. Xia, M. Billeter, P. Güntert, K. Wüthrich, The program XEASY for computer-supported NMR spectral-analysis of biological macromolecules, J. Biomol. NMR 6 (1995) 1–10.
[33] K. Wüthrich, NMR of Proteins and Nucleic Acids, pp. 30–31, 130–161, John Wiley and Sons, NY, 1986.
[34] C.A. Salgueiro, D.L. Turner, A.V. Xavier, Use of paramagnetic NMR probes for structural analysis in cytochromes c_3 from *Desulfovibrio vulgaris*, Eur. J. Biochem. 244 (1997) 721–734.
[35] P. Güntert, W. Braun, K. Wüthrich, Efficient computation of three-dimensional protein structures in solution from nuclear magnetic resonance data using the program DYANA and the supporting programs CALIBA, HABAS and GLOMSA, J. Mol. Biol. 217 (1991) 517–530.
[36] R. Boelens, T.M.G. Koning, R. Kaptein, Determination of biomolecular structures from proton–proton NOE's using a relaxation matrix approach, J. Mol. Struct. 173 (1988) 299–311.
[37] R. Boelens, T.M.G. Koning, G.A. van der Marel, J.H. van Boom, R. Kaptein, Iterative procedure for structure determination from proton–proton NOEs using a full relaxation matrix approach. Application to a DNA octamer, J. Magn. Reson. 82 (1989) 209–308.
[38] B.A. Borgias, T.L. James, Two-dimensional nuclear Overhauser effect: complete relaxation matrix analysis, Methods Enzymol. 176 (1989) 169–183.
[39] D.L. Turner, L. Brennan, H.E. Meyer, C. Lohaus, C. Siethoff, H.S. Costa, B. Gonzalez, H. Santos, J.E. Suárez, Solution structure of plantaricin C, a novel lantibiotic, Eur. J. Biochem. 264 (1999) 833–839.
[40] L. Brennan, D.L. Turner, A.C. Messias, M.L. Teodoro, J. LeGall, H. Santos, A.V. Xavier, Structural basis for the network of functional cooperativities in cytochrome c_3 from *Desulfovibrio gigas*: solution structures of the oxidised and reduced states, J. Mol. Biol. 298 (2000) 61–82.
[41] D.L. Turner, C.A. Salgueiro, P. Schenkels, J. LeGall, A.V. Xavier, Carbon-13 NMR studies of the influence of axial ligand orientation on haem electronic structure, Biochim. Biophys. Acta 1246 (1995) 24–28.
[42] R.O. Louro, I.J. Correia, L. Brennan, I. Coutinho, A.V. Xavier, D.L. Turner, Electronic structure of low-spin ferric porphyrins: ^{13}C NMR studies of the influence of axial ligand orientation, J. Am. Chem. Soc. 120 (1998) 13240–13247.
[43] D.L. Turner, R.J.P. Williams, ^{1}H- and ^{13}C-NMR investigation of redox-state-dependent and temperature-dependent conformation changes in horse cytochrome *c*, Eur. J. Biochem. 211 (1993) 555–562.
[44] R.S. Wareham, J.D. Kilburn, N.H. Rees, D.L. Turner, A.R. Leach, D.S. Holmes, Synthesis and solution conformation of a C_2 symmetric macrobicycle, Tetrahedron Lett. 36 (1995) 3047–3050.
[45] R.S. Wareham, J.D. Kilburn, D.L. Turner, N.H. Rees, D.S. Holmes, Homeomorphic isomerism in a peptidic macrobicycle, Angew. Chem., Int. Ed. 34 (1995) 2660–2662.
[46] D.L. Turner, L. Brennan, S.G. Chamberlin, R.O. Louro, A.V. Xavier, Determination of solution structures of paramagnetic proteins by NMR, Eur. Biophys. J. 27 (1998) 367–375.
[47] R. Koradi, M. Billeter, K. Wüthrich, MOLMOL: a program for display and analysis of macromolecular structures, J. Mol. Graphics 14 (1996) 51–55.
[48] R.A. Laskowski, J.A.C. Rullmann, M.W. MacArthur, R. Kaptein, J.M. Thornton, AQUA and PROCHECK-NMR: programs for checking the quality of protein structures solved by NMR, J. Biomol. NMR 8 (1996) 477–486.
[49] G. Vriend, WHAT IF: a molecular modeling and drug design program, J. Mol. Graphics 8 (1990) 52–56.
[50] E.G. Hutchinson, J.M. Thornton, PROMOTIF: a program to identify and analyse structural motifs in proteins, Protein Sci. 5 (1996) 212–220.
[51] A. Sofia, F. Oliveira, V.H. Teixeira, A.M. Baptista, C.M. Soares, Reorganization and conformational changes in the reduction of tetraheme cytochromes, Biophys. J. 89 (2005) 3919–3930.